MR-Less High Dimensional Spatial Normalization of ^{11}C PiB PET Images on a Population of Elderly, Mild Cognitive Impaired and Alzheimer Disease Patients

Jurgen Fripp[1], Pierrick Bourgeat[1], Parnesh Raniga[1,3], Oscar Acosta[1], Victor Villemagne[2], Gareth Jones[2], Graeme O'keefe[2], Christopher Rowe[2], Sébastien Ourselin[1,4], and Olivier Salvado[1]

[1] Australian e-Health Research Centre, CSIRO ICT Centre, Brisbane, Australia
[2] Department of Nuclear Medicine and Centre for PET, Austin Hospital, Melbourne, Australia
[3] School of Electrical and Information Engineering, The University of Sydney, Sydney, Australia
[4] (Current Affiliation) Centre for Medical Image Computing, University College London, London, United Kingdom

Abstract. $\beta - amyloid$ (Aβ) plaques are one of the neuropathological hallmarks of Alzheimer's disease (AD) and can be quantified using the marker ^{11}C PiB. As ^{11}C PiB PET images have limited anatomical information, an Magnetic Resonance Image (MRI) is usually acquired to perform the spatial normalization needed for population analysis. We designed and evaluated a high dimensional spatial normalization approach that only uses the ^{11}C PiB PET image. The non-rigid registration (NRR) is based on free form deformation (FFD) modelled using B-splines. To compensate for the limited anatomical information, the FFD is constrained to an allowable transform space using a model trained from MR registrations. Aβ deposition is dependent on disease staging, so a spatially normalized ^{11}C PiB PET appearance model selects and refines the atlas. The approach was compared with MR NRR using data from healthy elderly, mild cognitive impaired and Alzheimer disease participants. Using segmentation propagation, an average Dice similarity coefficient of 0.64 and 0.73 was obtained for white and gray matter. The R-squared correlation between the uptake obtained in the frontal, parietal, occipital and temporal was 0.789, 0.843, 0.871 and 0.964. These are very promising results, considering the low resolution of ^{11}C PiB PET images.

1 Introduction

$\beta - amyloid$ (Aβ) plaques are one of the neuropathological hallmarks of Alzheimer's disease (AD) and appear many years before cognitive symptoms become apparent. ^{11}C PiB PET [1] is one of the most promising imaging agents

D. Metaxas et al. (Eds.): MICCAI 2008, Part I, LNCS 5241, pp. 442–449, 2008.

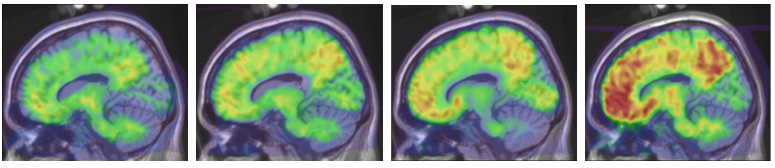

Fig. 1. Four example spatially normalized ^{11}C PiB PET cases overlaid on the Colin atlas *left* Healthy elderly *middle left* mild cognitive impaired *middle and far right* Alzheimer's

for assessing Aβ deposition. PiB has been shown to be more specific than other markers at binding to amyloid. In previous studies, it has been observed that the pattern of uptake found in ^{11}C PiB PET images can vary significantly and in some cases overlap between AD, mild cognitive impaired (MCI) and healthy elderly (NC). Example ^{11}C PiB PET images are presented in Fig. 1, which highlight this variability and indicate why high dimensional non-rigid registration is problematic.

Variation in brain structure and Aβ deposition between individuals, as well as differences in image resolution and field of view can make direct comparisons of ^{11}C PiB PET images difficult. To perform statistical analysis some form of spatial normalization is necessary. The standard approach is through linear scaling and non-linear warping, which is often performed using Statistical Parametric Mapping (SPM) [2]. This involves the patients ^{11}C PiB PET and MR being co-registered, the patients MR being affinely and non-rigidly warped to an atlas, then the warping is applied to the co-registered PET to obtain spatially normalized PET images [3,4]. The main disadvantages of this approach are the accumulation of registration errors and requiring an MR for each patient.

For future clinical use into the early detection of Alzheimers disease it is desirable to be able to analyse and compare ^{11}C PiB PET images accurately without requiring a MR image. There are several reasons why this is important: minimise the cost required for neurological assessment, reduce the burden on the patient and allow its implementation when MRs cannot be acquired (e.g. claustrophobic patients and/or metalic implants).

In some Fluorodeoxyglucose (FDG) and PiB PET studies, an average PET atlas has been used with linear and low dimensional warping [5,6,7]. However, ^{11}C PiB PET images exhibit highly variable and even non-corresponding regions of $\beta - amyloid$ deposition (often related to disease staging). Hence, the use of a single average atlas for ^{11}C PiB PET registration is not ideal and may adversely affect the registration results for some patients [7]. The use of a specifically selected atlas or a generated atlas that in some way best matches the participant's scan has been pursued in MR [8,9], and in many applications can allow more accurate non-rigid registration results [10]. In this paper we utilize a generative appearance model of spatially normalized ^{11}C PiB PET images to allow us to select and refine the atlas for each participant.

A popular approach for non-rigid registration is to use spline-based transformations [11]. In this paper the deformation is represented by a free form deformation (FFD) based on B-splines. Statistical control point model (SCPM) constraints can then be used to restrict these deformations to an allowable deformation space [12]. In general it has been found to improve robustness, although it can reduce precision. This is less of a concern for ^{11}C PiB PET images which have much lower resolution, higher noise and limited structural information compared to the MRs used to train the SCPM. We use SCPM in the non-rigid registration to provide constraints on the transformation model, and hence implicitly embed anatomical information.

We present an approach to perform MR-less ^{11}C PiB PET-PET spatial normalization. This is validated in a leave-one-out fashion on a large sample of real clinical participants from an Alzheimer study by comparing the spatial normalization obtained with that obtained using MR.

2 Method

2.1 Subjects

PiB PET scans from 98 participants enrolled in a longitudinal study assessing ^{11}C PiB PET for early diagnosis of AD were used in this study [13]. Participants were excluded if they were not fluent in English, mini-mental state examination (MMSE) was less than 12, or there was a history of brain injury or alcoholism. The 24 AD participants met NINCDS/ADRDA criteria for probable AD. The 20 MCI participants met Petersen's recently published consensus criteria. The remaining 54 participants were healthy elderly participants. Objective impairment was established as at least one neuropsychological test score falling 1.5 SD or more below relevant normative data.

2.2 Image Acquisition Protocols

The ^{11}C PiB PET scans were acquired using a Philips ADAC Allegro full-ring tomograph with PIZELAR germanium oxyorthosilicate crystal detectors. Each participant was injected with 370 MBq of ^{11}C-PiB and were scanned for 20 minutes starting 40 minutes post-injection. Summed images for the 40 to 60 minutes time frame were used (2x2x2mm). Sagittal MR images were acquired using a T_1 weighted 3D SPGR sequence 1.5T (1.1x1.1x1.5mm) and 3T scanners (0.5x0.5x2mm).

2.3 Registration for Training

The rigid PET to MR co-registration and MR to Atlas affine image registration was performed using the automated method of Ourselin et al [14]. This approach uses a block matching strategy to estimate the global transformation with a matching criteria of normalized cross correlation. The MR to atlas non-rigid registration was performed using an inhouse implementation of B-splines

based FFD [11]. The B-spline transformation model describing the deformation is written by the tensor product of the 1D cubic B-splines:

$$T_{local}(x,y,z) = \sum_{l=0}^{3}\sum_{m=0}^{3}\sum_{n=0}^{3} B_l(u)\, B_m(v)\, B_n(w)\, \phi_{i+l,j+m,k+n} \quad (1)$$

Where u, v and w are the relative positions of the index point along each axis and ϕ are the parameters of the B-splines. The matching criteria used in the FFD was normalized mutual information (NMI) [15], with the cost function $C_{total} = (1-\omega)C_{similarity} - \omega C_{constraint}$ where $C_{constraint}$ is the smoothness constraint from [16] with ω= 0.01. This was optimised in a three level multi-resolution scheme, with the image sub-sampled by a factor of 4, 2 and 1, and the control point spacing changed from 20, 10 to 5 mm respectively.

Using the aforementioned affine registration [14] and B-Spline based FFD [11] all participant's co-registered MR scans were spatially normalized to the Colin atlas [17]. The obtained transformations were then used to warp the participants ^{11}C PiB PET image to the Colin atlas and hence obtain spatially normalized ^{11}C PiB PET images. We will refer to this process as PET-MR spatial normalization, while the MR-less ^{11}C PiB PET spatial normalization approach will be referred to as PET-PET spatial normalization.

2.4 Principal Component Analysis

Given N images with M voxels we can construct a $X = M \times N$ matrix (each column i is the voxel data from the i th image x_i). Then the mean image is simply $\mu = \frac{1}{N}\sum_{i=1:N} x_i$. The principal component model was calculated using a singular value decomposition with the covariance matrix $\frac{1}{N}DD^T$ decomposed as $U\sum U^T = \frac{1}{N}DD^T$ where D is the mean-offset map (column i given by $D_i = x_i - \mu$), and U has column vectors that represent the orthogonal modes of variation and $\sum$ is a diagonal matrix of corresponding eigenvalues. An image x_{unseen} can be decomposed into a N dimensional vector of weights $w = U^T(x_{unseen} - \mu)$, which we will refer to as eigen-weights. Given eigen-weights w, an image x_{new} can be reconstructed by $x_{new} = Uw + \mu$. The principal component scores were constrained to be within 3 standard deviations.

Generative ^{11}C PiB PET Appearance Model: The ^{11}C PiB PET images was intensity normalized using a zero mean unit variance filter. Performing PCA on the intensity and spatially normalized ^{11}C PiB PET images allowed a generative appearance model to be created that could be used to generate intensity and spatially normalized ^{11}C PiB PET atlases. The number of modes used was 61 and accounted for 95% of the variation in the training data.

Statistical Control Point Model (SCPM): Performing PCA on the parameters ϕ of the B-spline obtained in the PET-MR spatial normalization allowed a SCPM to be computed for each level that was used to provide an allowable deformation space. This was used to constrain deformations to be close to those

previously seen in training. The number of modes used in each level was (84, 82, 79) and accounted for 95% of the variation in the training data.

2.5 PET-PET Spatial Normalization

The PET-PET spatial normalization approach extends SCPM constrained non-rigid registration to include the generative ^{11}C PiB PET appearance model. To initialize this approach, the original ^{11}C PiB PET image is affinely propagated to the Colin atlas. In this paper we want to directly compare the PET-MR and PET-PET spatial normalization, so the affine transformation obtained in training is used for both approaches, in practice a PET-PET affine registration would be used [7]. The initial atlas is generated using the affinely registered ^{11}C PiB PET image.

The PET-PET spatial normalization is then performed using the same FFD based non-rigid registration between the affinely registered ^{11}C PiB PET image and the generated atlas. This was performed in the same three level multi-resolution scheme with the same parameters used in the training. However, unlike the MR-PET spatial normalization, no smoothness constraints were used, instead every third iteration the current ϕ parameters were reconstructed (and constrained) using the SCPM. As well as this, the current atlas was refined every fifth iteration using the current spatially normalized ^{11}C PiB PET image with the generative appearance model. This approach tends to result in the appearance of the generated ^{11}C PiB PET atlas and the transformed ^{11}C PiB PET image becoming similar.

2.6 Validation

For validation we assume that the results obtained by the PET-MR spatial normalization is correct and treat it as ground truth. All experiments were performed in a leave one out fashion. The MRs were segmented into gray (GM), white matter (WM) and cerebral spinal fluid (CSF) [18]. The Dice similarity coefficient ($\text{DSC} = 2T_P/(2T_P + F_P + F_N)$, where T_P is true positive, T_N is true negative, F_P is false positive and F_N is false negative) was calculated between the propagated segmentations obtained using PET-MR and PET-PET spatial normalization. The mean uptake in various regions was also calculated for all images with the R-squared correlation calculated between the PET-PET (or affine) and MR-PET spatial normalization.

3 Results

Figure 2 qualitatively illustrates the typical spatial normalization. Qualitative assessment indicated that the PET-PET spatial normalization was very good, which was most evident in the ventricles, skull and outer cortex where more anatomical information is present. It was found that a realistic spatial normalization could **not** be obtained if only the generative atlas (using smoothness constraints) or SCPM (using mean spatially normalized ^{11}C PiB PET image as atlas) was used (results not shown).

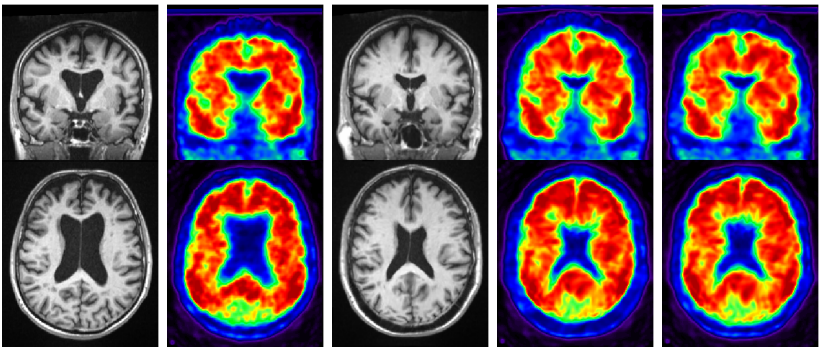

Fig. 2. Example registration results for one case *left to right* Affinely registered MR, Propagated Affinely Co-registered PiB, Non-rigidly registered MR, PET-MR spatial normalization and PET-PET spatial normalization

By propagating the GM, WM and CSF segmentation of each participant into the spatially normalized space, it can be seen (Figure 3) that the PET-PET approach is slightly inferior to MR-PET. By propagating the segmentations using the PET-MR and PET-PET spatial normalizations, an average DSC of 0.64 and 0.73 was obtained for the GM and WM. This is quite good, considering the average DSC for GM and WM obtained by comparing direct MR and ^{11}C PiB PET segmentation is 0.59 and 0.69 [19]. There was no obvious bias in the algorithm due to the disease staging, with all results similar in quality (Table 1). The minimum (and maximum) DSC for the GM, WM and CSF was 0.56 (0.69), 0.67 (0.78) and 0.40 (0.56).

In clinical studies, the primary interest is to extract statistics from various regions in the brain and to see whether changes in these regions are related to disease staging. So to further validate this approach we also consider the quantitative statistics obtained automatically from various regions (using composite regions defined with the AAL mask). An example of the average uptake (image

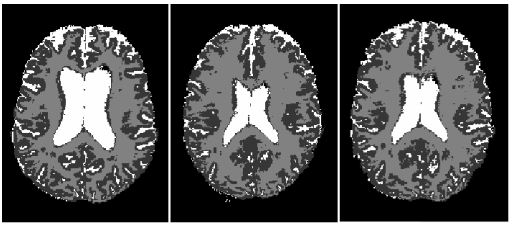

Fig. 3. Example GM, WM and CSF segmentation propagation using *left* Affine *middle* PET-MR and *right* PET-PET spatially normalization. This image illustrates the quality of the approach, with only minor errors in finer details, brain shape and ventricle size. **Note:** This is the same case and slice used in Figure 2.

Table 1. Mean (standard deviation) DSC results of the propagated segmentations on the spatially normalized atlas. The segmentation propogations were obtained using PET-MR and PET-PET transforms.

Class	GM	WM	CSF
AD	0.64 (0.02)	0.73 (0.02)	0.49 (0.04)
MCI	0.64 (0.02)	0.73 (0.02)	0.49 (0.04)
NC	0.65 (0.02)	0.74 (0.02)	0.49 (0.03)

Table 2. R-squared correlation between the uptake obtained in a region using PET-MR spatial normalization and the results of affine and our PET-PET spatial normalization

	Affine	PET-PET NRR
Frontal	0.726	0.789
Occipital	0.769	0.871
Parietal	0.779	0.843
Hippocampus	0.935	0.949
Precuneus	0.939	0.965
Temporal	0.952	0.964

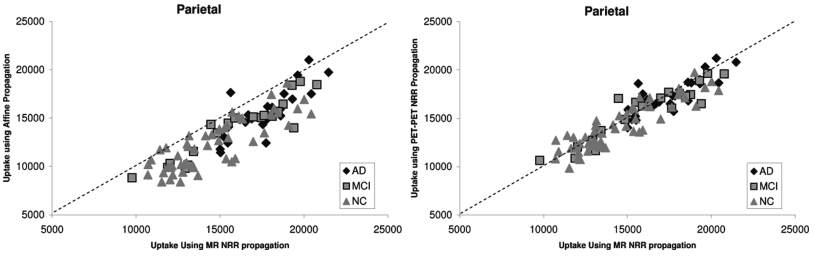

Fig. 4. Uptake found in the parietal region using MR spatial normalization compared to that found using *left* Affine and *right* PET-PET spatial normalization

intensity) in the parietal cortex is illustrated in Figure 4 by comparing affine and PET-PET to PET-MR. The R-squared correlation for several regions is also presented in Table 2, which show the close match between PET-PET and PET-MR spatial normalization, especially compared to the affine spatial normalization.

4 Conclusion

^{11}C PiB PET images could be spatially normalized with an accuracy almost as high as when using an MR scan, despite the limited anatomical resolution of the PET image. This was achieved by 1) constraining the approach to only use brain deformations that had been learn't from MR spatial normalization on a large database of MR scans, and 2) use a spatially normalized ^{11}C PiB PET atlas that was continually updated using a generative appearance model. This approach was validated using segmentation propagation and regional analysis and was shown to obtain results which are comparable to the traditional MR based spatial normalization, especially in regions where anatomical information is present (e.g. ventricles). The primary limitations of this approach are the computational cost ($\frac{1}{4}$, 1 and 5 hours for each respective level), requirement for significant training data and use of the same levels and control point spacing as the training data.

In conclusion, in the absence of MRs, it is possible to perform high dimensional spatial normalization of ^{11}C PiB PET image. This approach is relevant for widespread clinical use of amyloid imaging. Future work will involve refining this approach to include partial volume correction of the PiB PET images and to impose diffeomorphic constraints.

References

1. Klunk, W.E., et al.: Imaging brain amyloid in Alzheimer's disease with Pittsburgh Compound-B. Ann. Neurol. 55(3), 306–319 (2004)
2. Ashburner, J., et al.: Nonlinear Spatial Normalization Using Basis Functions. Human Brain Mapping 7, 254–266 (1999)
3. Ziolko, S., et al.: Evaluation of voxel-based methods for the statistical analysis of PIB PET amyloid imaging studies in Alzheimer's disease. NeuroImage 33(1), 94–102 (2006)
4. Lopresti, B., et al.: Simplified quantification of Pittsburgh Compound B amyloid imaging PET studies: a comparative analysis. J. Nucl. Med. 46(12), 1959–1972 (2005)
5. Lee, S., et al.: FDG-PET images quantified by probabilistic atlas of brain and surgical prognosis of temporal lobe epilepsy. Epilepsia (9), 1032–1038 (2002)
6. Kemppainen, N.M., et al.: PET amyloid ligand [11C] PIB uptake is increased in mild cognitive impairment. Neurology 68(19), 1603–1606 (2007)
7. Fripp, J., et al.: Generative atlases and atlas selection for C11-PIB PET-PET registration of Elderly. In: Mild cognitive impaired and Alzheimer disease patients IEEE Symp. on Biom. Imag., pp. 1155–1158 (2008)
8. Rohlfing, T., et al.: Evaluation of atlas selection strategies for atlas-based image segmentation with application to confocal microscopy images of bee brains. NeuroImage 21, 1428–1442 (2004)
9. Blezek, D., et al.: Atlas stratification. Med. Imag. Anal. 11(5), 443–457 (2007)
10. Wu, M., et al.: Optimum template selection for atlas-based segmentation. NeuroImage 34(4), 1612–1618 (2007)
11. Rueckert, D., et al.: Nonrigid registration using free-form deformations: Application to breast MR images. IEEE Trans. Med. Imag. 18, 712–721 (1999)
12. Rueckert, D., et al.: Automatic construction of 3-D statistical deformation models of the brain using nonrigid registration. IEEE Trans. Med. Imag. 8, 1014–1025 (2003)
13. Rowe, C.C., et al.: Imaging beta-amyloid burden in aging and dementia. Neurology 68(20), 1718–1725 (2007)
14. Ourselin, S., et al.: Reconstructing a 3D structure from serial histological sections. IVC 19, 25–31 (2001)
15. Studholme, C., et al.: An Overlap Invariant Entropy Measure of 3D Medical Image Alignment. Pattern Recognition 32(1), 71–86 (1999)
16. Rohlfing, T., et al.: Volume-preserving nonrigid registration of MR breast images using free-form deformation with an incompressibility constraint. IEEE Trans. Med. Imag. 22, 730–741 (2003)
17. Collins, D., et al.: Design and construction of a realistic digital brain phantom. IEEE Trans. Med. Imag. 17(3), 463–468 (1998)
18. Bourgeat, P., et al.: Improved cortical thickness measurement from MR images using partial volume estimation. In: IEEE Symp. on Biom. Imag., pp. 205–208 (2008)
19. Raniga, P., et al.: PIB-PET Segmentation for Automatic SUVR Normalization Without MR Information. In: IEEE Symp. on Biom. Imag., pp. 348–351 (2007)